# Supplementary materials for "Mixed dimensional transport in $CsV_3Sb_5$ single crystals"

Xiangwei Huang,¹ Chunyu Guo\*,¹ Carsten Putzke,¹ Yan Sun,² Maia G. Vergniory,².³ Ion Errea,³,4,5 Martin Gutierrez,⁴,6 Dong Chen,² Claudia Felser,² and Philip J. W. Moll†¹ ¹Laboratory of Quantum Materials (QMAT), Institute of Materials (IMX), École Polytechnique Fédérale de Lausanne (EPFL), CH-1015 Lausanne, Switzerland ²Max Planck Institute for Chemical Physics of Solids, 01187 Dresden, Germany ³Donostia International Physics Center, 20018 Donostia-San Sebastian, Spain ⁴Centro de Física de Materiales (CSIC-UPV/EHU), 20018 Donostia-San Sebastian, Spain ⁵Fisika Aplikatua Saila, Gipuzkoako Ingeniaritza Eskola, University of the Basque Country (UPV/EHU), 20018 Donostia-San Sebastian, Spain ⁶Department of Physics, University of the Basque

Country (UPV/EHU), Apartado 644, 48080 Bilbao, Spain

# I. ESTIMATION OF STRAIN DUE TO THERMAL CONTRACTION FOR MEM-BASED MI-CROSTRUCTURE

We now estimate the displacement applied to the sample from the thermal contraction of the  $SiN_x$  spring and the outer Si frame when cooling the device to cryogenic temperatures. The thermal contraction coefficient of  $SiN_x(\varepsilon_{SiN})$  and  $Si(\varepsilon_{Si})$  upon cooling from 300 K to 4 K are 0.0342% and 0.0208% respectively. Assuming the sample itself has a typical thermal contraction coefficient  $\varepsilon_{Samp} \approx 0.1\%$ , one can easily calculate the total thermal contraction of the  $SiN_x$  spring:

$$dL_{Samp} = L_{Samp} \times \varepsilon_{Samp} = 80 \ nm \tag{S1}$$

$$dL_{SiN} = L_{SiN} \times \varepsilon_{SiN} = 70 \ nm \tag{S2}$$

$$dL_{Si} = L_{Si} \times \varepsilon_{Si} = 60 \ nm \tag{S3}$$

$$dL_{total} = dL_{Samp} + dL_{SiN} - dL_{Si} = 90 nm$$
 (S4)

Since the spring constant of the  $SiN_x$  spring is determined as 110 N/m by Comsol multiphysics simulation, the pressure due to thermal contraction can be calculated as:

$$P_{samp} = k \cdot dL/A = 9.8 \, bar \tag{S5}$$

where A stands for the cross section of the spring.

#### II. DETAILS OF BAND STRUCTURE CALCULATIONS

First-principles density functional theory (DFT) calculations were performed using the Quantum Espresso package (QE)<sup>1</sup>. We used the generalized gradient approximation with the Perdew-Burke-Ernzerhof parameterization<sup>2</sup> together with projector-augmented wave pseudopotentials generated by Dal Corso<sup>3</sup>. In all cases, we used an energy cutoff of 90 Ry with a Methfessel-Paxton smearing<sup>4</sup> of 0.02 Ry. The structural relaxation was done with a 18x18x2 grid neglecting spin-orbit coupling (SOC) and was stopped when pressures are below 0.01 kBar. The bands and

the Fermi surface where computed with SOC and 18x18x12 and 25x25x16 respectively.

P. Giannozzi, O. Andreussi, T. Brumme, O. Bunau, M. B. Nardelli, M. Calandra, R. Car, C. Cavazzoni, D. Ceresoli, M. Cococcioni, N. Colonna, I. Carnimeo, A. D. Corso, S. de Gironcoli, P. Delugas, R. A. D. Jr, A. Ferretti, A. Floris, G. Fratesi, G. Fugallo, R. Gebauer, U. Gerstmann, F. Giustino, T. Gorni, J. Jia, M. Kawamura, H.-Y. Ko, A. Kokalj, E. Küçükbenli, M. Lazzeri, M. Marsili, N. Marzari, F. Mauri, N. L. Nguyen, H.-V. Nguyen, A. O. de-la Roza, L. Paulatto, S. Poncé, D. Rocca, R. Sabatini, B. Santra, M. Schlipf, A. P. Seitsonen, A. Smogunov, I. Timrov, T. Thonhauser, P. Umari, N. Vast, X. Wu, and S. Baroni, J. Phys. Condens. Mat. 29, 465901 (2017).

<sup>&</sup>lt;sup>2</sup> J. P. Perdew, K. Burke, and M. Ernzerhof, Phys. Rev. Lett. **77**, 3865 (1996).

<sup>&</sup>lt;sup>3</sup> A. Dal Corso, Comp. Mat. Sci. **95**, 337 (2014).

<sup>&</sup>lt;sup>4</sup> M. Methfessel and A. T. Paxton, Phys. Rev. B **40**, 3616 (1989).

## Mixed dimensional transport in CsV<sub>3</sub>Sb<sub>5</sub> single crystals

Xiangwei Huang,¹ Chunyu Guo\*,¹ Carsten Putzke,¹ Yan Sun,² Maia G. Vergniory,².³ Ion
Errea,³,4,5 Martin Gutierrez,⁴,6 Dong Chen,² Claudia Felser,² and Philip J. W. Moll†¹

¹Laboratory of Quantum Materials (QMAT), Institute of Materials (IMX),
École Polytechnique Fédérale de Lausanne (EPFL), CH-1015 Lausanne, Switzerland
²Max Planck Institute for Chemical Physics of Solids, 01187 Dresden, Germany
³Donostia International Physics Center,
20018 Donostia-San Sebastian, Spain
⁴Centro de Física de Materiales (CSIC-UPV/EHU),
20018 Donostia-San Sebastian, Spain
⁵Fisika Aplikatua Saila, Gipuzkoako Ingeniaritza Eskola,
University of the Basque Country (UPV/EHU),
20018 Donostia-San Sebastian, Spain
⁶Department of Physics, University of the Basque
Country (UPV/EHU), Apartado 644, 48080 Bilbao, Spain
(Dated: January 20, 2022)

#### **ABSTRACT**

The observation of superconductivity and charge order in the Kagome-net compound  $CsV_3Sb_5$  has raised interest in its possible topological superconducting state. Key to this puzzle, as in any structurally layered conductor, is its effective electronic dimensionality. Here we present transport evidence for its dual nature, the coexistence of high-mobility quasi-two-dimensional Fermi surface sheets with small closed pockets that are crucial for the overall mixed dimensionality of this metal. It reflects in an unusual complete vanishing of magnetoresistance above  $T_{CDW}$ , which increases by a factor of a million upon entering the ordered state. Quantum oscillations further confirm the presence of multiple, closed 3D pockets coexisting with the main cylinders - which take a central role in the out-of-plane transport. These results caution that the main Kagome physics may be altered when these planes are stacked in a real 3D material.

#### INTRODUCTION

When structurally layered materials host strong electronic correlations, their effective electronic dimensionality is key to understanding their microscopic physics. The anisotropic Fermi surface then sets the canvas on which correlated ground states unfold. Cuprate and pnictide hightemperature superconductors are prime examples of layered materials in which reduced dimensionality defines the superconducting state<sup>1,2</sup>. The anisotropy is further a critical parameter to describe the vortex formation and the orbital limit of the upper critical field. Recently, metals hosting planes with Kagome nets have attracted significant attention due to their topological phases as well as potential correlation effects<sup>3–5</sup>. The latter have been argued to arise from small-bandwidth bands (flat bands) that are predicted in phenotypical two-dimensional Kagome models<sup>6</sup>. Flat bands naturally enhance correlation effects when the Coulomb energy exceeds the kinetic energy and they lead to a divergent density of state, an entropic catastrophe materials commonly avoid by forming electronically ordered states at low temperatures. However, when in multiband systems the flat bands coexist with other, dispersive bands, screening counteracts such mechanisms. When idealized Kagome planes are stacked to form a three-dimensional crystal, their out-of-plane coupling determines the degree of hybridization, the effective dimensionality and thereby how much Kagome physics survives.

The stacked Kagome structure of CsV<sub>3</sub>Sb<sub>5</sub> [Fig. 1(a) and (b)] presents an ideal testbed to in-

vestigate the dimensionality of such systems, and its influence on the rich physics it hosts such as the topologically non-trivial band structure, superconductivity and charge-density-wave (CDW) order. The Kagome nets are formed by V atoms, and their stacking results in a topological  $Z_2$  metal<sup>5,7-9</sup>. Its overall band structure, including multiple bulk Dirac points, has been determined by angle-resolved photoemission spectroscopy (ARPES)<sup>7,10</sup>. Upon cooling, the Kagome lattice undergoes a CDW transition at  $T_{CDW} = 93 \text{ K}^{11-13}$ . A 2×2 reconstruction on the Kagome plane as well as a three dimensional  $2\times2\times2$  ordering are readily observed by scanning tunneling microscopy (STM)<sup>13,14</sup>. At even lower temperatures of  $T_c \sim 2.8 \text{ K}$ , superconductivity appears<sup>7</sup>. The non-trivial band topology may give rise to topological superconductivity. Indeed, scanning tunneling microscopy has uncovered a zero-bias peak in the vortex cores which, while not conclusive, is compatible with a scenario of bound Majorana states<sup>13</sup>. Here we show that  $CsV_3Sb_5$  is a distinctly three-dimensional material, despite its layered structure. Both the normal state resistivity anisotropy and quantum oscillations support a picture of strong interlayer coupling and three-dimensionality.

#### **RESULTS**

The single-particle band structure from ab-initio calculations serves as a starting point to investigate the dimensionality of this strongly correlated compound. The electronic structure of  $CsV_3Sb_5$  in the high-symmetry state is calculated by density functional theory (DFT) using the Quantum Espresso package (QE)<sup>15</sup>. An energy cutoff of 90 Ry is used with a Methfessel-Paxton smearing <sup>16</sup> of 0.02 Ry. Multiple bands are found at the Fermi level [Fig. 1(c)], consistent with the previous reports<sup>5</sup>. Accordingly, multiple Fermi surfaces of either cylindrical or ellipsoidal shape are expected in the Brillouin zone [Fig. 1(d)]. While the layered structure is reflected in the electron-like cylinders centered at  $\Gamma$  and K, their sizable dispersion signals pronounced interlayer coupling. In absence of spin-orbit coupling (SOC), the cylinder at the Brillouin zone boundary (H to K) would surround a nodal line, yet SOC breaks this degeneracy in the real material. Meanwhile a small pocket at the L-point encloses a symmetry-protected Dirac node. The complex multi-band structure of  $CsV_3Sb_5$  is characterized by pronounced out-of-plane dispersion, and hence suggests significant coupling between the Kagome planes.

This electronic dimensionality can be experimentally probed via the resistivity anisotropy. As common in structurally layered materials, the CsV<sub>3</sub>Sb<sub>5</sub> crystals grow as thin platelets aligned

with the Kagome plane<sup>5</sup>. While this crystal morphology lends itself to in-plane resistivity measurements, quantitative out-of-plane transport poses a well-known challenge. Focused Ion Beam (FIB) milling can be used to prepare micron-sized crystalline bars with well-defined geometries to quantify the resistivity<sup>17</sup>. However, thermal mismatch strain on microstructures is inevitable<sup>18</sup>, which has been shown to strongly alter the correlated landscape of  $CsV_3Sb_5^{19,20}$  and readily cleave such layered materials. We address this issue through a novel type of soft coupling of a microstructured sample to a supportive frame via a patterned  $SiN_x$  membrane [Fig. 1(e)]. The main idea is to suspend the patterned crystal (purple) in free space, only connecting it mechanically to a substrate by patterned microsprings (golden).

The fabrication starts by cutting a cross-sectional slice of the platelet in the ac-plane by FIB milling. A Xe-ion beam is used to avoid ion implantation, and a low-voltage polish step at 5 kV reduces the amorphization layer into the nm-range<sup>21</sup>. This slab is then transferred to a commercial SiN<sub>x</sub> transmission electron microscopy window (SPI). The  $500\times500~\mu m$  wide window in a Si frame is spanned by a 200 nm thin membrane. After Au-evaporation, the sample is further patterned into a symmetric transport geometry and the remaining window is cut into a meandering spring, to further soften the mount guided by finite element simulations. We have fabricated both in-plane and out-of-plane aligned microbars that are maximally decoupled from its mechanical support[Fig. 1(f)]. They feature a minimal residual pressure that allows to probe reliably transport bars of materials which easily cleave ( $\approx 9.8$  bar, see supplement).

The in-plane resistivity decreases from  $80~\mu\Omega$ cm at 300K to  $0.3~\mu\Omega$ cm at  $T_c=2.7$  K. The high residual resistivity ratio (RRR) of 250 is larger compared to bulk samples<sup>22</sup>, evidencing the high quality of the microstructure fabrication (Fig. 2). The in-plane resistivity displays a small yet sharply defined discontinuity at the CDW transition at  $T_{CDW}$ . The out-of-plane resistivity,  $\rho_c$ , is significantly higher yet shows an overall similar metallic temperature dependence. It decreases from  $\rho_c(300\text{K}) \sim 1.9~\text{m}\Omega$ cm to  $\rho_c(T_c) \sim 33~\mu\Omega$ cm, corresponding to a lower RRR of 60 for the out-of-plane transport. Unlike the in-plane resistivity,  $\rho_c$  shows an upwards jump at  $T_{CDW}$  [Fig. 2(c)], evidencing a stronger impact of the CDW formation on the out-of-plane transport compared to the in-plane one. These results are qualitatively reflected in the challenging measurements of  $\rho_c$  on bulk crystals<sup>7</sup>, yet deviate quantitatively. The substantially larger RRR in the microstructures suggests that our devices are closer to the intrinsic bulk value. Accordingly, the jump of  $\rho_c$  at  $T_{CDW}$  is more prominent (  $(\rho_c(T_{CDW}^+) - \rho_c(T_{CDW}^-))/\rho_c(T_{CDW}^+) \approx 12\%$ ).

This enhanced impact of the density wave on transport suggests the low-strain mounting to

be a promising route to probe the intrinsic transport modification due to the CDW formation. At high temperatures above  $T_{CDW}$ , the picture of a moderately anisotropic metal with an almost temperature-independent anisotropy emerges  $(\rho_c/\rho_{ab}(T=300K)\approx 24)$ . This value falls close to the Fermi velocity anisotropy of 20 when averaged over the entire Fermi surface [Fig. 2(d)]. Given that the lifetime may well be k-dependent and the phonon spectrum certainly reflects the crystalline anisotropy, this close match suggests that the material is indeed about as anisotropic as the Fermi surface suggests.

Upon entering into the CDW state, the transport anisotropy increases sharply from 31.5 to 38, reflecting the upward jump in  $\rho_c$  and downward one in  $\rho_{ab}$ . This suppressed interlayer transport is a natural result of a band reconstruction along the c-direction as in a  $2\times2\times2$  order suggested by a  $\pi$  phase shift of the CDW across an atomic step edge recently observed by STM<sup>13</sup>. Further lowering the temperature increases the anisotropy which eventually saturates around 100 at  $T_c$ . This high value suggests that transport at low temperatures is indeed dominated by the inplane electronic system in the distorted Kagome planes, however the robustly metallic behavior and moderate value of  $\rho_c(T_c) \sim 33~\mu\Omega cm$  signal a three-dimensional electronic system. Taking the first-order derivative of the resistivity anisotropy reveals further, more subtle changes in the material [Fig. 2(e)]. Besides the clear spike at  $T_{CDW}$ , a local minimum occurs at around 70 K. This temperature coincides with the onset of anisotropy in the muon spin depolarization rate that has been associated with the onset of time-reversal-symmetry breaking (TRSB)<sup>23</sup>. The TRSB state has been theoretically proposed to arise from an effective orbital current loop flux<sup>24</sup>, and a modification of a magnetic scattering channel would be a natural connection between this experiment and ours.

The magnetoresistance can further refine this transport picture (Fig. 3). The first non-trivial observation comes from the complete absence of transverse magnetoresistance for orthogonal inplane fields and currents at any temperature above  $T_{CDW}$ . The field-independent noise floor provides an upper bound for the magnetoresistance, at  $\Delta \rho_a(18T)/\rho_a(0T) < 10^{-5}$  at 140 K. Even rather unsuspicious metals such as Cu commonly show transverse magnetoresistances around 1% (20T) at room temperature and 100% (20T) at 100K, following the increase of the quasiparticle lifetime  $\tau$  with decreasing temperature<sup>25</sup>. Here, with a complex Fermi surface and incipient TRSB order, such flat magnetoresistance is quite exotic. This behavior changes abruptly at  $T_{CDW}$ , below which a sizable magnetoresistance is uncovered. This behavior is further anisotropic, as all other orthogonal current-field configurations show a weak magnetoresistance compatible with normal

metals.

The transverse magnetoresistance at various temperatures can be more quantitatively analyzed by Kohler scaling, which holds when the magnetoresistance is fully explained by orbital effects with a field-independent scattering rate<sup>26</sup>. Conversely, its failure indicates a field-dependence of the scattering time or a temperature dependence of the Fermi surface. The former is commonly observed through the field-polarization of magnetic scattering in magnetic materials, while the latter appears in density wave systems due to the temperature-dependence of the single-particle gap<sup>27</sup>. As expected, CsV<sub>3</sub>Sb<sub>5</sub> violates Kohler scaling at any temperature, with a clear deviation of the curves at  $T_{CDW}$ . The unusual absence of magnetoresistance for currents in the ab-direction and fields in the a-direction is further apparent as a pathological Kohler scaling, as all data is merely noise around zero. At lowest temperatures, a consistent picture of large magnetoresistance emerges, compatible with open orbits in the in-plane direction. Semiclassical magnetotransport effects are scaled by  $\omega_c \tau$ , with  $\tau$  the carrier lifetime and  $\omega_c = eB/m^*$  the cyclotron frequency. One scenario for the absence of magnetoresistance is the dirty limit ( $\tau \sim 0$ ), such that laboratory fields never reach meaningful values of  $\omega_c \tau$ . This scenario is clearly at odds with the low inplane resistivity and the emergence of quantum oscillations at low fields. An alternative scenario is an extremely clean quasi-2D electronic system, for which no magnetoresistance is expected in this open-orbit configuration. This implies that the cylindrical FS sheets completely short-circuit the other complex 3D-like segments. Interestingly this scenario is compatible with the transport anisotropy.

This poses severe questions about the fate of the small, 3D-like pockets and the overall dimensionality of the material. Four low frequency quantum oscillation have been observed for out-of-plane fields and associated with these small 3D pockets<sup>11,28</sup>. However, these quantum oscillations quickly disappear when the field is rotated to the in-plane directions. As ellipsoidal and cylindrical Fermi surfaces only meaningfully differ in quantum oscillations close to the in-plane field direction, the true electronic dimensionality was not established. The improved quality and cleanliness of the strain-free bars now allows us to track this frequency over the entrie angle range, firmly establishing them as closed 3D pockets within the density wave phase (Fig. 4). The angular dependence of oscillation frequencies is well described by a simple ellipsoidal model  $F_i \propto 1/\sqrt{\sin^2(\theta) + (1+A_i^2)\cos^2(\theta)}$  we obtained the anisotropic factor  $A_i$  which characterizes the Fermi surface anisotropy for each ellipsoidal Fermi surfaces with i the index of them [Fig. 4(d)].

In conclusion, the electronic anisotropy and Fermiology of  $CsV_3Sb_5$  exhibit a surprising coexistence of a high-mobility in-plane electronic system coexisting with small 3D pockets, explaining the coherent transport in the out-of-plane direction. This decoupling manifests itself in the complete absence of in-plane magnetoresistance under crossed in-plane fields. The out-of-plane restructuring at the  $2\times2\times2$  density wave transition,  $T_{CDW}$ , restores a sizable magnetoresistance in all directions. This is compatible with the observation of closed, 3D-like pockets in quantum oscillations. These results establish  $CsV_3Sb_5$  as a conductor of mixed dimensionality, and theoretical models based on simplified 2D Kagome lattices may miss important aspects of this material.

#### REFERENCES

- <sup>1</sup> J. G. Bednorz and K. A. Müller, Z. Phys. B Condens. **64**, 189 (1986).
- <sup>2</sup> Y. Kamihara, H. Hiramatsu, M. Hirano, R. Kawamura, H. Yanagi, T. Kamiya, and H. Hosono, J. Am. Chem. Soc. **128**, 10012 (2006).
- <sup>3</sup> T. Kida, L. Fenner, A. Dee, I. Terasaki, M. Hagiwara, and A. Wills, J. Condens. Mat. Phys. **23**, 112205 (2011).
- <sup>4</sup> M. Kang, S. Fang, L. Ye, H. C. Po, J. Denlinger, C. Jozwiak, A. Bostwick, E. Rotenberg, E. Kaxiras, J. G. Checkelsky, et al., Nat. Commun. 11, 4004 (2020).
- <sup>5</sup> B. R. Ortiz, L. C. Gomes, J. R. Morey, M. Winiarski, M. Bordelon, J. S. Mangum, I. W. Oswald, J. A. Rodriguez-Rivera, J. R. Neilson, S. D. Wilson, et al., Phys. Rev. Mater. **3**, 094407 (2019).
- <sup>6</sup> A. O'Brien, F. Pollmann, and P. Fulde, Phys. Rev. B **81**, 235115 (2010).
- <sup>7</sup> B. R. Ortiz, S. M. Teicher, Y. Hu, J. L. Zuo, P. M. Sarte, E. C. Schueller, A. M. Abeykoon, M. J. Krogstad, S. Rosenkranz, R. Osborn, et al., Phys. Rev. Lett. **125**, 247002 (2020).
- <sup>8</sup> Y. Fu, N. Zhao, Z. Chen, Q. Yin, Z. Tu, C. Gong, C. Xi, X. Zhu, Y. Sun, K. Liu, and H. Lei, Phys. Rev. Lett. 127, 207002 (2021).
- <sup>9</sup> D. Chen, B. He, M. Yao, Y. Pan, H. Lin, W. Schnelle, Y. Sun, J. Gooth, L. Taillefer, and C. Felser, arXiv:2110.13085 (2021).
- Y. Luo, S. Peng, S. M. Teicher, L. Huai, Y. Hu, B. R. Ortiz, Z. Wei, J. Shen, Z. Ou, B. Wang, et al., arXiv:2106.01248 (2021).
- <sup>11</sup> F. Yu, T. Wu, Z. Wang, B. Lei, W. Zhuo, J. Ying, and X. Chen, Phys. Rev. B **104**, L041103 (2021).
- <sup>12</sup> C. Mu, Q. Yin, Z. Tu, C. Gong, H. Lei, Z. Li, and J. Luo, Chin. Phys. Lett. **38**, 077402 (2021).
- <sup>13</sup> Z. Liang, X. Hou, F. Zhang, W. Ma, P. Wu, Z. Zhang, F. Yu, J.-J. Ying, K. Jiang, L. Shan, et al., Phys. Rev. X 11, 031026 (2021).
- <sup>14</sup> H. Zhao, H. Li, B. R. Ortiz, S. M. Teicher, T. Park, M. Ye, Z. Wang, L. Balents, S. D. Wilson, and I. Zeljkovic, Nature 599, 216 (2021).
- P. Giannozzi, O. Andreussi, T. Brumme, O. Bunau, M. B. Nardelli, M. Calandra, R. Car, C. Cavazzoni, D. Ceresoli, M. Cococcioni, N. Colonna, I. Carnimeo, A. D. Corso, S. de Gironcoli, P. Delugas, R. A. D. Jr, A. Ferretti, A. Floris, G. Fratesi, G. Fugallo, R. Gebauer, U. Gerstmann, F. Giustino, T. Gorni, J. Jia,

- M. Kawamura, H.-Y. Ko, A. Kokalj, E. Küçükbenli, M. Lazzeri, M. Marsili, N. Marzari, F. Mauri,
- N. L. Nguyen, H.-V. Nguyen, A. O. de-la Roza, L. Paulatto, S. Poncé, D. Rocca, R. Sabatini, B. Santra,
- M. Schlipf, A. P. Seitsonen, A. Smogunov, I. Timrov, T. Thonhauser, P. Umari, N. Vast, X. Wu, and S. Baroni, J. Phys. Condens. Mat. **29**, 465901 (2017).
- <sup>16</sup> M. Methfessel and A. T. Paxton, Phys. Rev. B **40**, 3616 (1989).
- <sup>17</sup> P. J. W. Moll, Annu. Rev. Condens. Mat. Phys. **9**, 147 (2018).
- M. D. Bachmann, N. Nair, F. Flicker, R. Ilan, T. Meng, N. J. Ghimire, E. D. Bauer, F. Ronning, J. G. Analytis, and P. J. W. Moll, Sci. Adv. 3, e1602983 (2017).
- <sup>19</sup> B. Song, X. Kong, W. Xia, Q. Yin, C. Tu, C. Zhao, D. Dai, K. Meng, Z. Tao, Z. Tu, et al., arXiv:2105.09248 (2021).
- <sup>20</sup> F. Du, S. Luo, B. R. Ortiz, Y. Chen, W. Duan, D. Zhang, X. Lu, S. D. Wilson, Y. Song, and H. Yuan, Phys. Rev. B 103, L220504 (2021).
- <sup>21</sup> R. Kelley, K. Song, B. Van Leer, D. Wall, and L. Kwakman, Microsc. Microanal. **19**, 862 (2013).
- <sup>22</sup> Y. Xiang, Q. Li, Y. Li, W. Xie, H. Yang, Z. Wang, Y. Yao, and H.-H. Wen, Nat. Commun. **12**, 6727 (2021).
- <sup>23</sup> L. Yu, C. Wang, Y. Zhang, M. Sander, S. Ni, Z. Lu, S. Ma, Z. Wang, Z. Zhao, H. Chen, et al., arXiv:2107.10714 (2021).
- <sup>24</sup> X. Feng, K. Jiang, Z. Wang, and J. Hu, Sci. Bull. **66**, 1384 (2021).
- <sup>25</sup> J. De Launay, R. Dolecek, and R. Webber, J. Phys. Chem. Solids **11**, 37 (1959).
- <sup>26</sup> J. M. Ziman, Electrons and phonons: the theory of transport phenomena in solids (2001).
- N. Maksimovic, I. M. Hayes, V. Nagarajan, J. G. Analytis, A. E. Koshelev, J. Singleton, Y. Lee, and T. Schenkel, Phys. Rev. X 10, 041062 (2020).
- <sup>28</sup> B. R. Ortiz, S. M. Teicher, L. Kautzsch, P. M. Sarte, J. P. Ruff, R. Seshadri, and S. D. Wilson, Phys. Rev. X 11, 041030 (2021).

### Acknowledgements

**Funding:** This work was funded by the European Research Council (ERC) under the European Union's Horizon 2020 research and innovation programme (MiTopMat - grant agreement No. 715730). This project received funding by the Swiss National Science Foundation (Grants No. PP00P2\_176789). M.G.V., I. E. and M.G.A. acknowledge the Spanish Ministerio de Ciencia e Innovacion (grant PID2019-109905GB-C21). M.G.V. thanks support to Programa Red Guipuzcoana de Ciencia Tecnología e Innovación 2021 No. 2021-CIEN-000070-01 Gipuzkoa Next and the Deutsche Forschungsgemeinschaft (DFG, German Research Foundation) GA 3314/1-1 – FOR 5249 (QUAST). This work has been supported in part by Basque Government grant IT979-16. This work was also supported by the European Research Council Advanced Grant (No. 742068) "TOPMAT", the Deutsche Forschungsgemeinschaft (Project-ID No. 258499086) "SFB 1143", and the DFG through the Würzburg-Dresden Cluster of Excellence on Complexity and Topology in Quantum Matter ct.qmat (EXC 2147, Project-ID No. 39085490).

**Competing Interests** The authors declare that they have no competing financial interests.

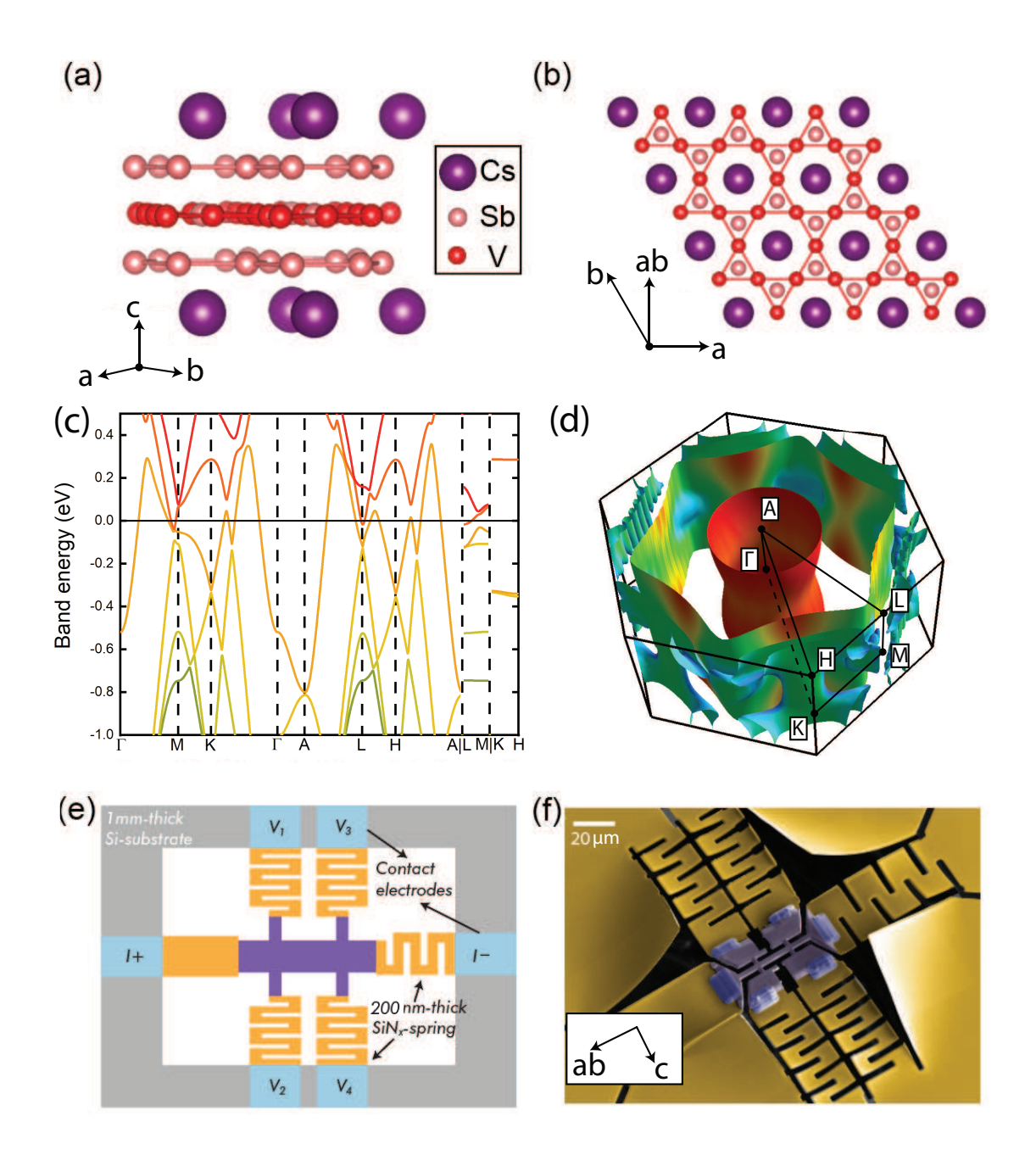


FIG. 1. Side(a) and top(b) view of crystal structure of  $CsV_3Sb_5$ . It consists with layers of Cs, V and Sb atoms which form the Kagome lattice plane. (c) Electronic structure of  $CsV_3Sb_5$  calculated by density functinal theory. There exist multiple electronic bands across the Fermi level. (d) Fermi surfaces in the Brillouin zone, including several types of Fermi surfaces and their symmetric copies. (e) Illustration of membrane-mount  $CsV_3Sb_5$  device. The sample is suspended with soft  $SiN_x$  springs, which ensures the minimum strain effect. (f) Scanning-electron-microscope (SEM) image of the Membrane device. The 250 by 250  $\mu$ m membrane window was patterned into several branches of springs with FIB.

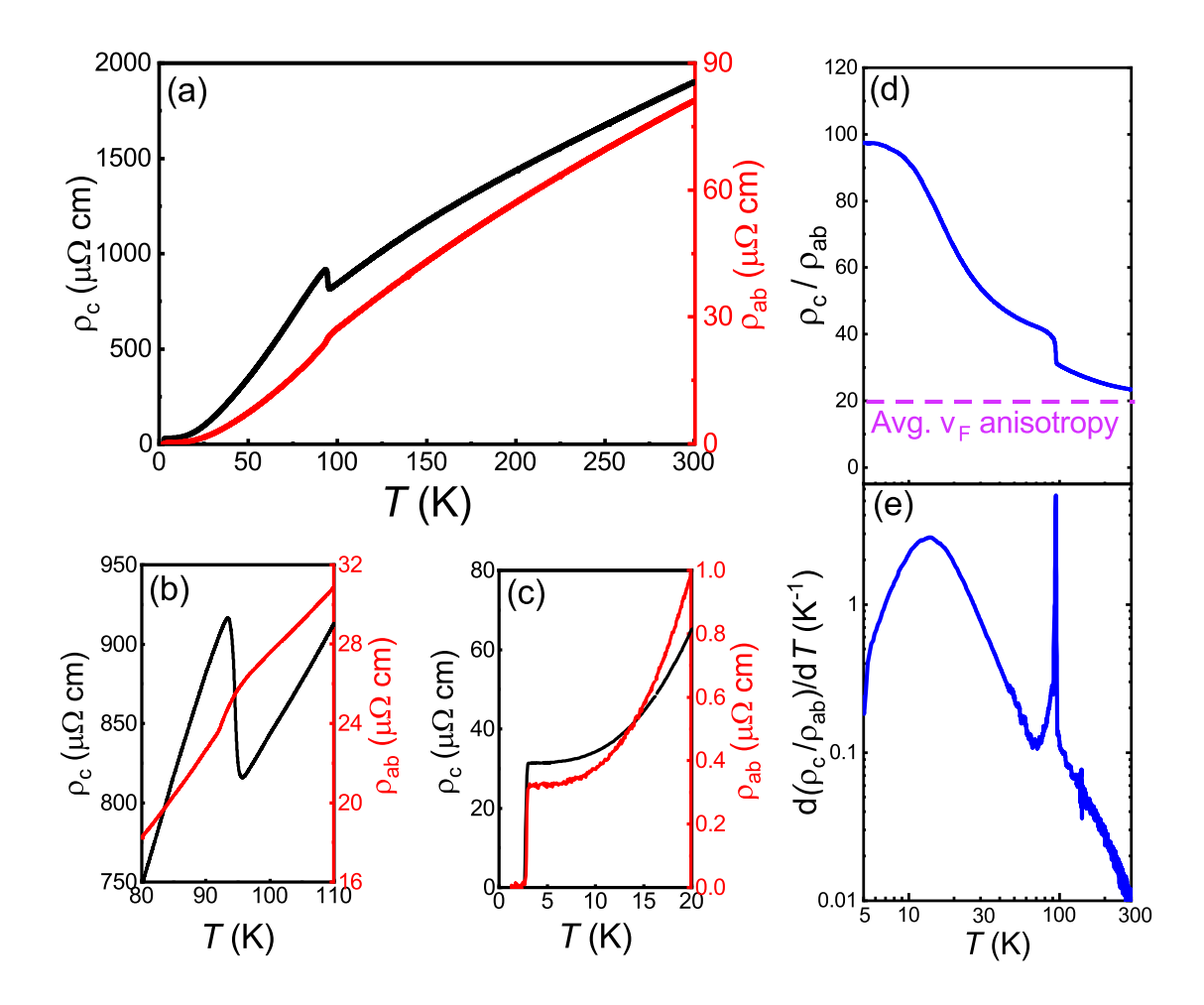


FIG. 2. (a) Temperature dependence of the out-of-plane( $\rho_c$ ) and in-plane resistivity( $\rho_{ab}$ ). (b) An abrupt jump occurs in the temperature dependence of  $\rho_c$ , which corresponds to the charge-density-wave transition temperature  $T_{CDW}$ . Consistently  $\rho_{ab}$  also displays a weak discontinuity. (c) Enlarged view of (a) within the low temperature range which demonstrates a clear superconducting transition at  $T_c = 2.8$  K. (d) Temperature dependence of resistivity anisotropy ( $\rho_c/\rho_{ab}$ ). The dashed lines stand for the averaged Fermi velocity anisotropy for all Fermi surfaces. (e) First-order derivative of temperature dependence of resistivity anisotropy [d( $\rho_c/\rho_{ab}$ )/dT]. At the charge-density-wave transition temperature ( $T_{CDW}$ ) a sharp peak can be observed, as well as a broad hump at T"  $\approx 14$  K.

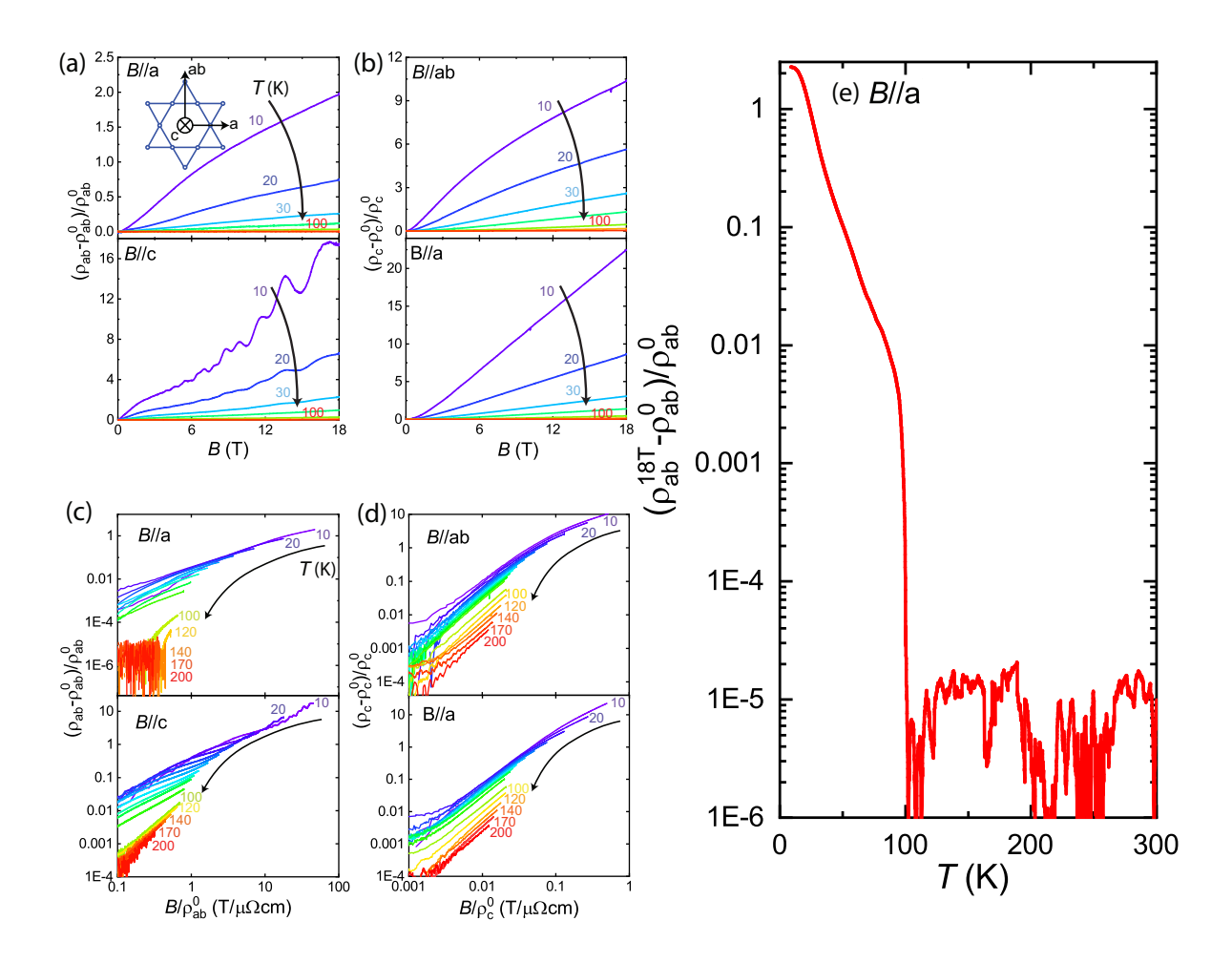


FIG. 3. Field dependence of out-of-plane (a) and in-plane (b) magnetoresistance ratio  $[(\rho - \rho^0)/\rho^0]$  with field applied along a and c-axis. (c) and (d) stand for Kohler's scaling plot of in-plane and out-of-plane magneto-resistivity respectively. (e) Temperature dependence of magnetoresistance ratio at B=18 T with current along ab-axis and field along a-axis which are defined in the inset of (a).

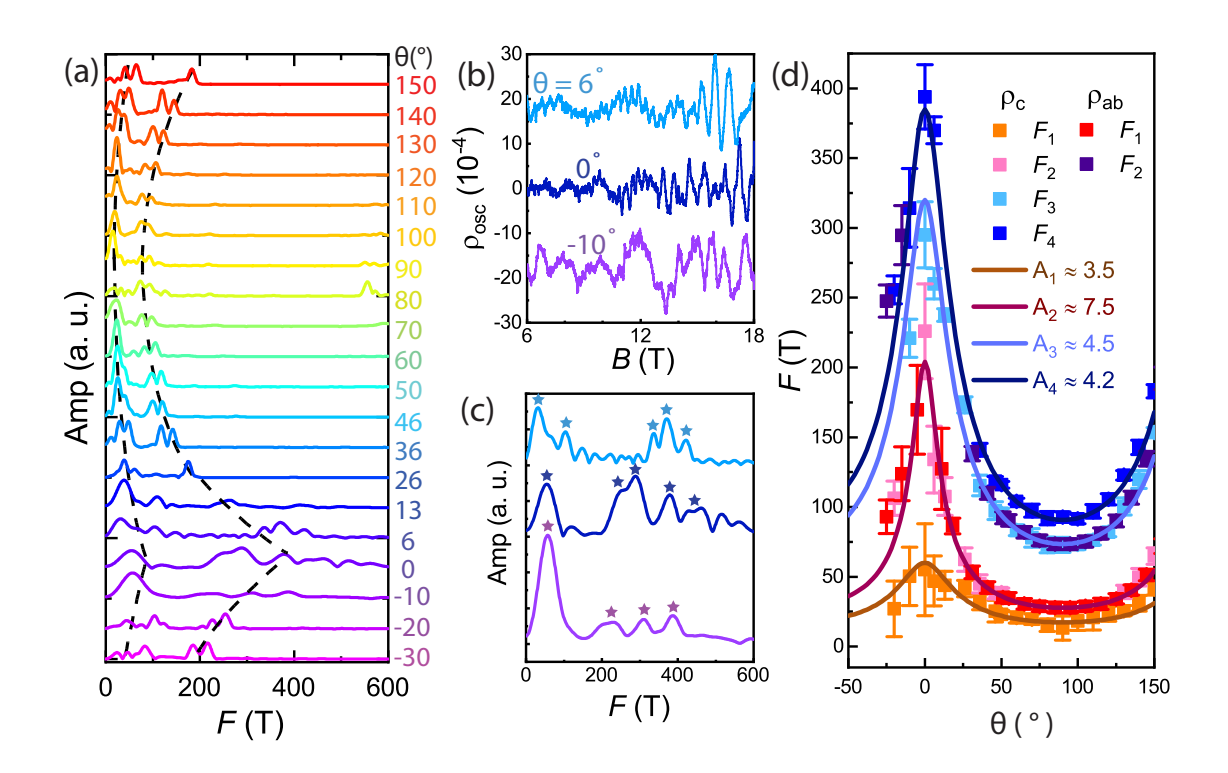


FIG. 4. (a) Fast-Fourier-transformation(FFT) spectrum with different field directions for Shubnikov-de-Hass(SdH) oscillations measured with current applied along c-axis. Here  $\theta$  stands for the angle between a-axis and field direction. (b) SdH oscillations ( $\rho_{osc}$ ) at  $\theta$  = 6, 0 and -10°. Here  $\rho_{osc} = \Delta \rho/\rho_{BG}$ , with  $\Delta \rho$  the oscillatory part of the magneto-resistivity, and  $\rho_{BG}$  a polynomial fit to the magneto-resistivity background. (c) Corresponding FFT spectrum with the star symbols indicate the identified peaks. (d) Angular dependence of SdH oscillation frequencies. The error bar is defined as full width at half maximum of the peaks in the FFT spectrum.